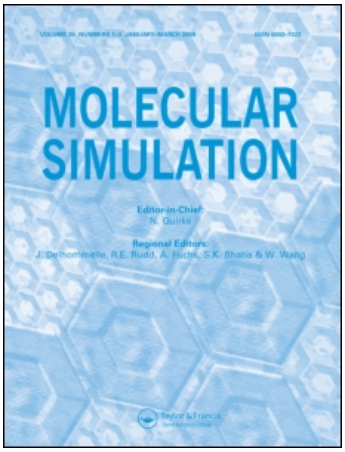

Molecular Simulation
Publication details, including instructions for authors and subscription information:
http://www.informaworld.com/smpp/title~content=t713644482

The Depletion Attraction between Pairs of Colloid Particles in Polymer Solution

Alberto Striolo[a]; Coray M. Colina[a]; Keith E. Gubbins[a]; Nicola Elvassore[b]; Leo Lue[c]
[a] Department of Chemical Engineering, North Carolina State University, Raleigh, NC, USA [b] Dipartimento di Principi e Impianti di Ingegneria Chimica, Universita' di Padova, Padova, Italy [c] Department of Chemical Engineering, University of Manchester Institute of Science and Technology, Manchester, United Kingdom

To cite this Article Striolo, Alberto , Colina, Coray M. , Gubbins, Keith E. , Elvassore, Nicola and Lue, Leo(2004) 'The Depletion Attraction between Pairs of Colloid Particles in Polymer Solution', Molecular Simulation, 30: 7, 437 — 449
To link to this Article: DOI: 10.1080/0892702042000197649
URL: http://dx.doi.org/10.1080/0892702042000197649

Molecular Simulation, Vol. 30 (7), 15 June 2004, pp. 437–449

Taylor & Francis
Taylor & Francis Group

The Depletion Attraction between Pairs of Colloid Particles in Polymer Solution

ALBERTO STRIOLO[a,*], CORAY M. COLINA[a], KEITH E. GUBBINS[a], NICOLA ELVASSORE[b] and LEO LUE[c]

[a]*Department of Chemical Engineering, North Carolina State University, 113 Riddick Labs, Raleigh, NC 27695, USA;* [b]*Dipartimento di Principi e Impianti di Ingegneria Chimica, Universita' di Padova, Via Marzolo 9, 35100 Padova, Italy;* [c]*Department of Chemical Engineering, University of Manchester Institute of Science and Technology, P.O. Box 88, Sackville Street, Manchester M60, 1QD, United Kingdom*

(Received April 2003; In final form December 2003)

NVT Monte Carlo simulations were used to assess the effective interaction between pairs of colloid particles dissolved in non-adsorbing polymer solutions. The polymers were represented as freely-jointed-hard-sphere chains composed of 10, 20, or 30 segments. The size of the interacting colloid particles was similar to or smaller than the radius of gyration of the polymers.

Results show a short-range colloid–colloid depletion attraction. At low polymer concentration, this attraction slowly decays to zero at increasing separations. At higher polymer concentration, the depletion attraction is coupled to a mid-range repulsion, especially for solutions of short, stiff polymers. From the simulated forces, osmotic second virial coefficients were computed for colloids as a function of polymer concentration. The calculated osmotic second virial coefficients exhibit a non-monotonic dependence on polymer concentration, in qualitative agreement with experimental results.

The simulated colloid–colloid potentials of mean force were used, within a perturbation theory, to calculate fluid–fluid and fluid–solid coexistence curves. The colloids are treated as a pseudo one-component system, and the polymers in solution are considered only through the effective pair potential between the dissolved colloids. When long flexible polymers are dissolved in solution, the phase diagram for small colloid particles shows a fluid–fluid coexistence curve at low colloid packing fraction, and a fluid–solid coexistence curve at higher packing fraction. As the size of the colloid particles increases, the molecular weight of the polymer decreases, or the polymer concentration in solution increases, the fluid–fluid coexistence curve becomes metastable with respect to the fluid–solid coexistence curve.

Keywords: Potential of mean force; Polymer flexibility; Phase diagrams; Colloid particles

INTRODUCTION

Many industrial processes, particularly in the food and biotechnology industries, manufacture solutions containing polymers and other globular particles. Despite the wide and multidisciplinary interest that surrounds colloid–polymer systems, much still remains to be understood before a general theoretical description can be attempted [1]. The appeal of understanding and predicting the thermodynamic properties of these systems stems from economical and technological reasons, and also from the challenge of describing multi-component solutions in which large rigid bodies are dissolved with long flexible polymers.

Previous theoretical and experimental studies were dedicated to solutions containing large colloids and small polymers (i.e. the colloidal limit) [2]. Asakura and Oosawa [3,4] introduced the idea of depletion attraction between large colloid particles dissolved in polymer solutions in 1954. Their thermodynamic model predicts a colloid–colloid attraction that increases with increasing osmotic pressure of the polymer solution and decreases with increasing colloid–colloid separation. These theoretical expectations were verified only in the 1980s, when it was experimentally proved that adding non-adsorbing polymers to a colloidal solution may cause the flocculation of the colloidal particles [5,6]. Joanny *et al.* [7] showed that as the polymer concentration increases the range of colloid–colloid interaction becomes of the order of magnitude of the correlation length of the polymer solution, less than the radius of

*Corresponding author. Present Address: Department of Chemical Engineering, Vanderbilt University, 118 Olin Hall, Nashville, TN 37235-1604, USA. Tel.: +1-615-322-8793. Fax: +1-615-343-7951. E-mail: alberto.striolo@vanderbilt.edu

ISSN 0892-7022 print/ISSN 1029-0435 online © 2004 Taylor & Francis Ltd
DOI: 10.1080/0892702042000197649

gyration of the polymers. Mean field theories suggested that as the polymer concentration increases the depletion attraction becomes too weak to induce phase separation [8].

More recently, theoretical and experimental investigations have been concentrated on colloidal solutions containing polymers whose radius of gyration is similar to or larger than the radius of the colloids (i.e. the protein limit). For example, Yethiraj *et al.* [9] demonstrated that a short-range colloid–colloid depletion attraction may be associated with a mid-range effective repulsion. Paricaud *et al.* [10] examined the segment/colloid diameter ratio at which fluid–fluid demixing occurs as a function of the chain length of the polymer, and they proposed that demixing is due to the enthalpy rather than the entropy of mixing.

Among available experimental studies, Ye *et al.* [11] examined the depletion interaction between $CaCO_3$ particles diluted in solutions of polyisoprene in decane. Their results showed that the range of the colloid–colloid depletion attraction decreases with increasing polymer concentration and that the colloid–colloid attraction at contact increases with increasing polymer concentration until it reaches a maximum. Poon [12] recently presented a detailed review of the work done on solutions containing PMMA colloids and polystyrene. When PMMA colloids are dissolved in hydrocarbon solvents, they behave as hard spheres. As polystyrene is added to the system, the colloidal fluid–crystal coexistence region is expanded compared to that of the pure hard-sphere system for small polymer/colloid size ratios, but a three-phase coexistence of colloidal gas, liquid, and crystal phases is observed for large polymer/colloid size ratios [13]. Kulkarni *et al.* [14–17] studied aqueous protein/polymer solutions and isolated the contribution of the depletion interaction to the effective protein–protein potential of mean force. They showed that the depletion attraction follows a non-monotonic behavior with increasing polymer concentration, and that the minimum of the osmotic second virial coefficient is reached at lower polymer concentrations as the polymer molecular weight is increased.

At present, molecular-level investigations are required to fully understand the effect of polymer length, stiffness, and architecture on the effective colloid–colloid potential of mean force. Within the McMillan-Mayer level of description [18], once the colloid–colloid interaction potential is known, several theories could be used to obtain densities and structures of coexisting phases [19]. For example, Gast *et al.* [20] applied a second-order perturbation theory to predict the phase diagram for colloidal particles in polymer solutions. The model qualitatively reproduced experimental results by de Hek and Vrij [5], but predicted a fluid–solid rather than a fluid–fluid phase separation. Previous simulation studies focused on the colloidal limit [21], where the effective pair interaction is predominantly attractive. Louis *et al.* [22] reported lattice simulation results for colloidal pairs interacting in solutions containing polymers described as 100-segments-long self-avoiding walks. Dzubiella *et al.* [23] reported integral equation, computer simulations, and phase-equilibria calculations for the colloid–colloid depletion interaction when colloids are in solution with star polymers. Both Louis *et al.* [22] and Dzubiella *et al.* [23] represented the interacting polymers as soft spheres, hence their results were predicted by the Asakura-Oosawa model. In a recent work [24], Bolhuis *et al.* presented fluid–fluid phase diagrams, obtained from lattice simulations, in the protein limit for colloids dissolved in interacting and non-interacting polymers. Their results indicate a polymer-mediated depletion attraction between pairs of colloids in solution that decays with increasing colloid–colloid separation.

In this work, we use off-lattice molecular-simulation techniques in the canonical (NVT) ensemble [25] to study the colloid–colloid interaction potential generated by the presence of non-adsorbing polymers in solution. The systems simulated consist of pairs of colloid particles interacting in model polymer solutions. Polymers are represented as freely-jointed-hard-sphere chains and are characterized by different flexibility. All interactions other than excluded-volume are neglected. Because of computational limitations, solvent molecules are not explicitly considered, and consequently results reported for colloid–colloid forces are to be considered averaged over the polymer configurations and the solvent-molecule displacements. The simulated colloid–colloid potentials of mean force are used to compute osmotic second virial coefficients for colloids in polymer solutions and to predict fluid–fluid and fluid–solid phase equilibria. In partial agreement with available experimental data, the calculated osmotic second virial coefficients exhibit a non-monotonic dependence on polymer concentration. We discuss the effect of polymer concentration, polymer molecular weight, and colloidal size on the features of the global phase diagrams for colloids in polymer solutions.

SIMULATION METHOD

The colloid–polymer systems simulated consist of pairs of hard-sphere colloid particles interacting

in a box containing freely-jointed-hard-sphere-chain polymers. Polymers of various flexibilities are obtained by varying the ratio between the polymer-segment diameter (σ) and the separation between consecutive segments in a polymer chain (l). A polymer is flexible when σ is less than l and rigid when σ is larger than l. Simulations were conducted within the canonical (NVT) Monte Carlo ensemble using this off-lattice model. The number of particles, the volume of the simulation box, and the temperature remained constant throughout the simulation. A cubic box was considered and periodic boundary conditions implemented. The simulation-box size was at least three times larger than the radius of gyration of the polymers. The largest system studied contains 230 polymers of 30 segments each in a box of dimension $32l$.

During a simulation run the colloids positions were maintained fixed while polymer chains were allowed to move. Trial moves included polymer translations and pivot moves. The translation vector was automatically adjusted to give fifty percent acceptance probability. Polymer conformation changes were obtained with the pivot algorithm [26]. To improve computational efficiency, the Verlet neighbor-list algorithm was implemented [27]. Trial moves were accepted or rejected according to the Metropolis algorithm [25]. Initial configurations were obtained first by displacing the two colloids at the desired center-to-center separation, and then by building each polymer chain within the box up to the desired concentration.

At every center-to-center separation, the effective colloid–colloid force was computed following the method of Wu *et al.* [28]. The polymer-segment density was computed around the pair of interacting colloid particles. A virtual plane, that cuts the simulation box along the main diagonal, was divided into smaller boxes, and the probability to find a polymer segment in each box was computed. A typical equilibration run was about 0.2 billion (2×10^8) trial-moves long, while a production run was at least 2 billion (2×10^9) trial-moves long. For selected systems, the center of mass of polymers randomly chosen among the population was followed during a typical production run. At the conditions chosen, it was verified that polymers are free to move across the simulation box, except in those regions not accessible due to colloid–polymer excluded-volume effects.

Isolated polymer conformations were generated using the ensemble-growth algorithm [29,30] to obtain the polymer radius of gyration at infinite dilution. An ensemble of 10,000 polymer chains was considered for each polymer built. Results for the radius of gyration squared reported in Table I are the average of five runs (see Ref. [31] for details).

TABLE I Results obtained for the sample-averaged radius of gyration squared ($\langle R_g^2\rangle$) for the polymers considered in this work

σ/l	N	$\langle R_g^2\rangle/l^2$	q
0.4	20	4.06 ± 0.02	0.80
0.8	20	6.21 ± 0.04	0.99
1.0	10	2.85 ± 0.01	0.68
1.0	20	7.30 ± 0.06	1.08
1.0	30	12.35 ± 0.13	1.41
1.2	20	8.47 ± 0.05	1.16

Angular brackets denote sample-averaged results. σ/l is the ratio between the polymer-segment hard-sphere diameter and the separation between consecutive segments in a polymer chain. N is the number of segments in the polymer chain. q is the ratio between the radius of gyration of the polymer and the radius of the colloid when $D = 5l$. When q equals 0.68 results here reported are not in the protein limit.

SIMULATED COLLOID–COLLOID INTERACTIONS

Results presented are discussed in terms of polymer-segment number density ($\rho_P l^3$) computed as:

$$\rho_P l^3 = N n_p \frac{1}{V_{box}} l^3, \quad (1)$$

where N is the number of segments in a polymer chain, n_p is the number of polymer chains in the simulation box, and V_{box} is the simulation-box volume.

Results obtained for the colloid–colloid force when the interacting colloids (IC) are in solution with small hard spheres (SHS) are shown in Fig. 1 as a function of the reduced center-to-center separation r/D. Results presented in Fig. 1 satisfactorily reproduce those reported by Dickman *et al.* [32]. The ratio between the diameter of the colloids (D) and that of the SHS equals 5 and the SHS number density is 0.225. As shown in Fig. 1, the ICs experience a depletion attraction at short separations, coupled with repulsion at intermediate separations. The repulsion is due to accumulation of SHS in the region between the interacting colloids (Fig. 2). In fact, SHS accumulate at short distances from the ICs. While for $r/l = 5.2$ (Fig. 2a) the region between the colloids shows a depletion of SHS, at $r/l = 6.0$ (Fig. 2b) there is a significant accumulation of SHS between the ICs. The depletion of SHS between the colloids generates an effective colloid–colloid attraction, while the accumulation of SHS determines the repulsion.

Results for the colloid–colloid forces when the ICs are dissolved in polymer solutions are also shown in Fig. 1. Polymers considered were 10-, 20- and 30-segments long. The features of the colloid-colloid force profile change significantly when the SHS are

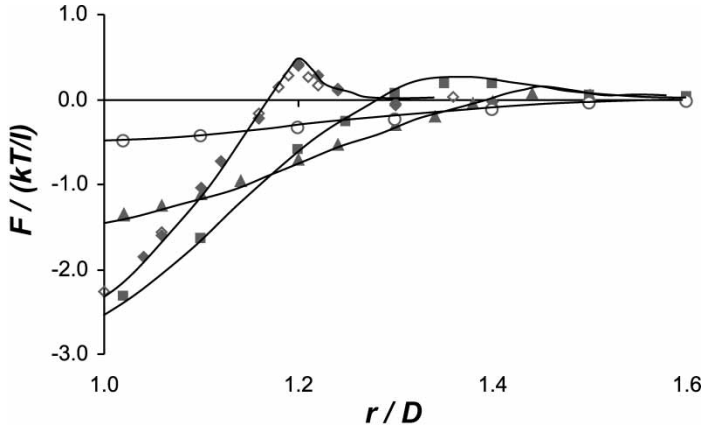

FIGURE 1 Effective colloid–colloid force between pairs of $D = 5l$ colloids interacting in polymer solutions. Diamonds are for colloids in $\rho_P l^3 = 0.225$ solution of small hard spheres (solid symbols are results from this work, open symbols are from Dickman *et al.* [32]). Squares are for colloids in $\rho_P l^3 = 0.30$ solution of 10-segments-long polymers, triangles are for colloids in $\rho_P l^3 = 0.225$ solution of 20-segment-long polymers, and circles are for colloids in $\rho_P l^3 = 0.10$ solution of 30-segment-long polymers. In all cases, $\sigma/l = 1.0$. Lines are guides for the eye.

connected to form polymers. The intensity of both the attractive force at contact and of the mid-range repulsion seems to decrease, while the range of the colloid–colloid depletion interaction increases. As predicted by the Asakura-Oosawa model, the depletion attraction at contact scales with the osmotic pressure of polymers in solution [3,4]. The osmotic pressure depends on the number density of molecules, which decreases when the SHS are connected to form polymers at fixed polymer-segment volume fraction. In addition, a non-adsorbing polymer is repelled from a hard surface for entropic reasons (see, for example, Ref. [33] and references therein), thus the attractive colloid–colloid force at contact is lower when the SHS are connected forming polymers than when they are free in solution. However, it should be noted that the depletion force at contact does not scale linearly with the concentration of polymers. The results in Fig. 1 also show that as the polymer length increases, the colloid–colloid repulsion decreases and is shifted to larger separations because of excluded-volume effects. In fact, for entropic reasons polymers are excluded from the region between the ICs and the force profile cannot show mid-range colloid–colloid repulsion when the polymers are sufficiently large. The range of polymer-mediated colloid–colloid depletion attraction depends on the size of polymers in solution, thus it is longer for larger polymers.

Results for the effective colloid–colloid force when the ICs are in solution with 20-segment-long polymers characterized by different stiffness (σ/l ratios) are shown in Fig. 3. The polymer-segment number density equals 0.225 and the diameter of the colloids is $5l$. Polymer-colloid size ratios $q = R_g/R_C$ (where R_C is the radius of the colloid) are included in Table I. The colloid–colloid depletion attraction at contact increases with increasing polymer stiffness because flexible polymers are more strongly repelled from hard surfaces compared to stiff polymers. Also, as the polymer stiffness increases, the mid-range repulsion rises. When $\sigma < l$, no colloid–colloid repulsion is obtained at the considered polymer-segment number density, and the colloid–colloid depletion attraction gradually decreases in intensity and reaches zero asymptotically. However, when $\sigma = l$, a very weak colloid–colloid repulsion is obtained at a reduced center-to-center distance (r/D) of about 1.5. In qualitative agreement with theoretical calculations for colloid-rod solutions [34], when $\sigma = 1.2l$, the colloid–colloid repulsion at $r/D \sim 1.3$ becomes significantly large. This unexpectedly large repulsion is probably due to the fact that stiff polymers may be trapped in the region between the interacting colloids. The range of colloid–colloid attraction increases with polymer stiffness because the polymer radius of gyration increases accordingly (see Table I). The results shown in Fig. 3 qualitatively agree with theoretical calculations for the effective pair potential of mean force for colloids dissolved in rod solutions [35]. In fact, even small amounts of rods in solution could generate significant colloid–colloid mid-range repulsions [35] that may be the cause of the stabilization of several metastable states observed in colloidal science [36].

Polymer-segment density profiles around a pair of interacting colloids in solutions containing 20-segment-long polymers when $D = 5l$ and $\sigma = l$ for $\rho_P l^3 = 0.225$ are shown in Fig. 4 at $r/l = 5.1$ (Fig. 4a) and 6.0 (Fig. 4b). The polymer-segment density around the colloids, and in particular in the region between the ICs, is less than the bulk average; hence the colloid–colloid effective interaction is attractive.

Polymer-segment density profiles around a pair of ICs are shown in Fig. 5 for colloids dissolved in 20-segment-long, $\rho_P l^3 = 0.225$, $\sigma = 1.2l$ polymer solutions. At $r/l = 5.1$ (Fig. 5a), the depletion regions of the two colloids overlap, and an effective attraction

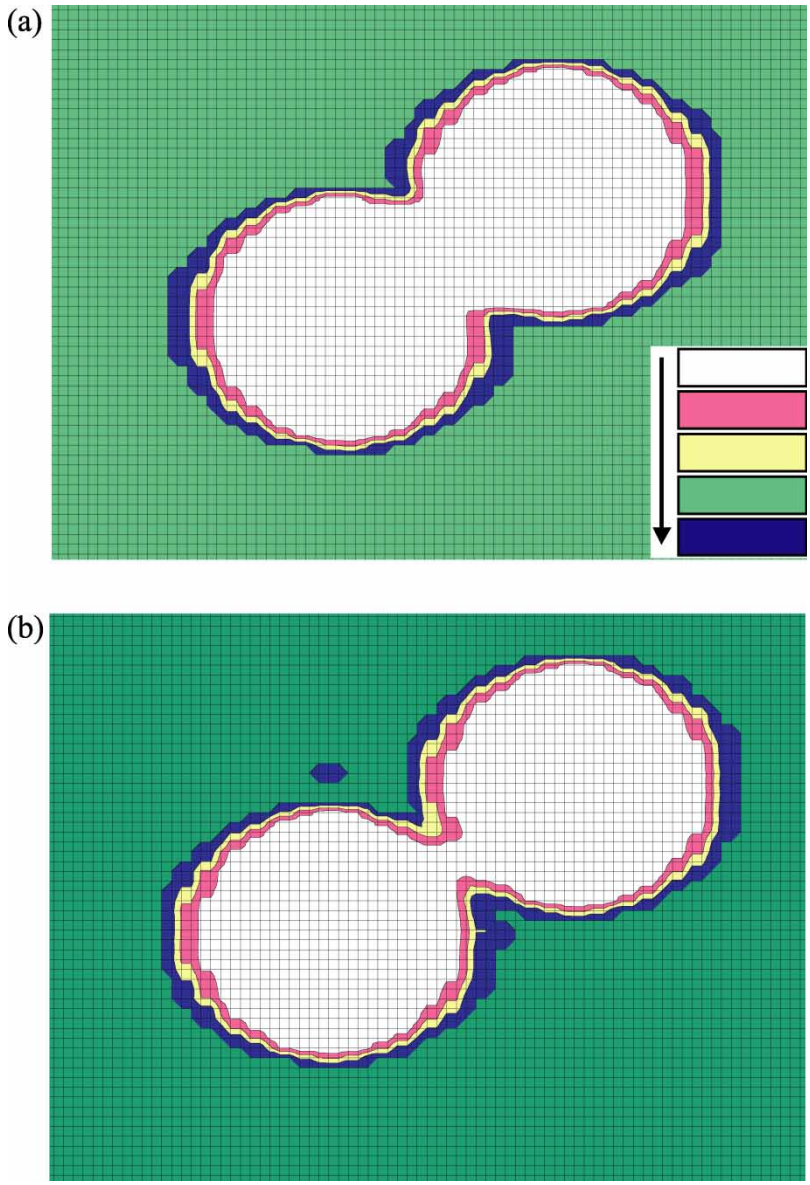

FIGURE 2 Small-hard-sphere density profiles around the pair of interacting colloids at center-to-center separation $r/l = 5.2$ (a) and $r/l = 6.0$ (b). Different colors represent different surface densities in the range $0 \div 0.046$, $0.046 \div 0.092$, $0.092 \div 0.138$, $0.138 \div 0.184$, $0.184 \div 0.230$ segments$/l^2$, as graphically illustrated in the inset. Conditions are those for Fig. 1. (Colour version available online.)

arises as discussed earlier (Figs. 2a and 4a). At $r/l = 7.0$ (Fig. 5b), the segment-density profile indicates that the depletion regions are beginning to overlap; nevertheless some regions of higher polymer-segment density can be identified between the interacting colloids. As a consequence, the colloid–colloid interaction at that separation is repulsive, as shown in Fig. 3. At $r/l = 8.0$ (Fig. 5c), the depletion regions around the ICs do not overlap, and the colloids no longer interact with each other.

Results obtained for the polymer-mediated colloid–colloid force for ICs dissolved in 20-segment-long polymer solutions at different polymer concentrations are shown in Fig. 6. Polymers of different stiffness are considered. Figure 6a is for $\sigma = l$ and Fig. 6b is for $\sigma = 1.2l$; the colloid diameter is $D = 5l$ in both cases. As the polymer concentration increases, the depletion force at contact increases because the osmotic pressure of the polymer solution increases. Our results show that for both polymers, the range of the depletion attraction decreases as the polymer concentration increases, and that mid-range repulsion arises. The peak of the colloid–colloid repulsion is shifted at shorter separations as the polymer concentration increases. While the repulsion is not significant for $\sigma = 1.0l$ at all polymer concentrations considered, it becomes unexpectedly marked for $\sigma = 1.2l$ and $\rho_P l^3 = 0.30$, probably because stiff polymers may be trapped between the ICs (see Fig. 5). Our results qualitatively agree with experimental observations according to which colloidal solutions flocculate at low polymer concentration due to depletion attraction, but may be stable at higher polymer concentrations due to

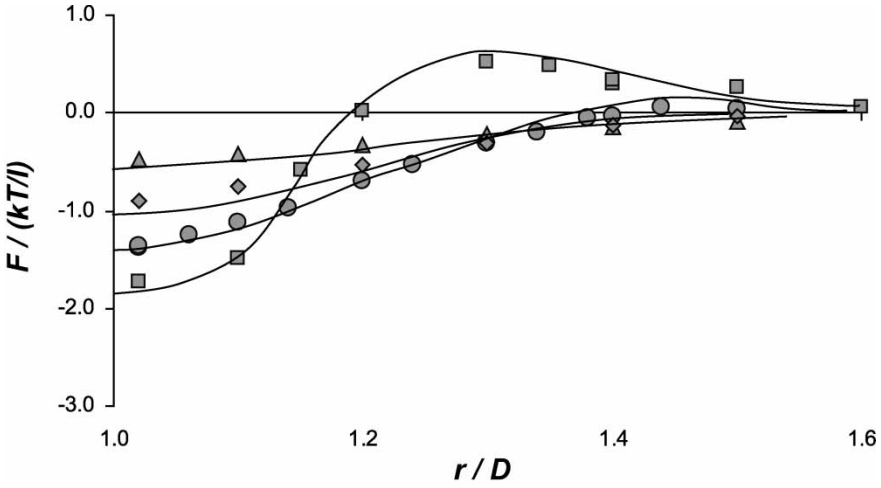

FIGURE 3 Colloid–colloid force as a function of center-to-center separation for pairs of colloids in $\rho_P l^3 = 0.225$, 20-segment-long polymer solutions. Polymers of different stiffness are considered. Squares are for $\sigma/l = 1.2$, circles are for $\sigma/l = 1$, diamonds are for $\sigma/l = 0.8$, and triangles are for $\sigma/l = 0.4$. Lines are guides for the eye.

short-range attraction coupled with mid-range repulsion [35–38].

From numerical integration of the simulated force profiles, it is possible to obtain the polymer-mediated colloid–colloid potential of mean force $W^{\text{pol}}_{\text{simulated}}$ as a function of separation. The contribution due to polymer-mediated interactions of the second osmotic virial coefficient (B^{pol}) can be obtained as:

$$B^{\text{pol}} = 2\pi \int_1^\infty \tilde{r}^2 \left(1 - \exp\left[\frac{-W^{\text{pol}}_{\text{simulated}}(\tilde{r})}{kT}\right]\right) \mathrm{d}\tilde{r} \qquad (2)$$

where k is the Boltzmann constant, T is the absolute temperature, and $\tilde{r}$ is the reduced colloid–colloid center-to-center separation r/D. Negative B^{pol} indicates an effective colloid–colloid two-body attraction, while positive B^{pol} indicates an effective colloid–colloid repulsion. Results for the colloid–colloid osmotic second virial coefficient B (obtained summing the hard-sphere contribution $2/3\pi D^3$ to B^{pol}) as a function of polymer-segment number density are shown in Fig. 7 for $D = 5l$ colloids dissolved in 20-segment-long polymer solutions with $\sigma = l$ or $\sigma = 1.2l$. For both cases, our results indicate that low concentrations of polymers in solution reduce the hard-sphere repulsion between colloids. However, if the polymer concentration is increased, B^{pol} becomes positive (especially when $\sigma = 1.2l$). At larger concentrations, our results suggest that the osmotic second virial coefficient may become negative (especially for $\sigma = 1.0l$), inducing an effective attraction between interacting colloids. Results shown in Fig. 7 are in qualitative agreement with theoretical predictions by Tuinier *et al.* [39], and by Chatterjee and Schweizer [40], and could partially explain results for the osmotic second virial coefficient for proteins in aqueous polymer solutions that show a minimum as the polymer concentration is increased [14–17]. However, it should be stressed that our calculations intentionally neglect important colloid–colloid and colloid–polymer interactions (electrostatic and hydrophobic interactions, preferential adsorptions of polymers, solvent effects, etc.) that may also be responsible for the non-monotonic dependence of the osmotic second virial coefficient on the concentration of polymers in solution.

Results for the polymer-mediated colloid–colloid force when colloids of different sizes are dissolved in solutions of 20-segment-long, $\sigma = 1.2l$, $\rho_P l^3 = 0.10$ polymers are shown in Fig. 8. At the conditions considered, simulation results do not provide evidence of colloid–colloid repulsion, but only of polymer-mediated depletion attraction. Our results indicate that the depletion force at contact is larger for large colloid particles. The reason for this result may be two-fold. Firstly, when larger colloid particles are dissolved in a simulation box of fixed volume, the volume available to polymer chains is reduced, thus the effective polymer concentration and the osmotic pressure increase. Secondly, the probability to find polymer segments in the region between the ICs is lower when large colloid particles are approaching than when small ones are, hence the depletion attraction is larger. It should also be noted that results in Fig. 8 indicate that the range of polymer-mediated depletion attraction increases significantly as the size of the colloid particles decreases.

PREDICTED PHASE DIAGRAMS AND DISCUSSION

Within the McMillan-Mayer level of description [18], colloid–polymer–solvent systems are

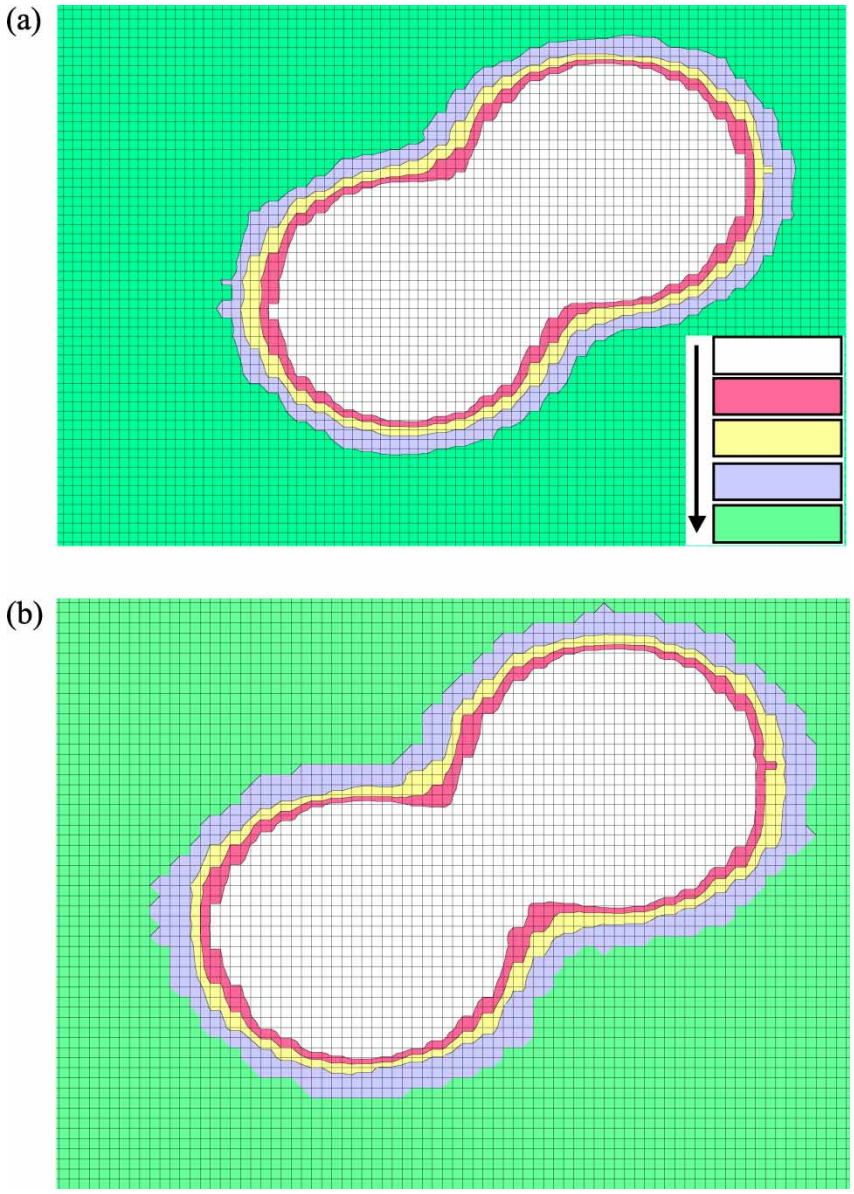

FIGURE 4 Polymer-segment density profiles around the interacting pairs of colloids at two colloid–colloid center-to-center separations $r/l = 5.1$ (a) and $r/l = 6.0$ (b). Different colors represent different surface densities in the range $0 \div 0.046$, $0.046 \div 0.092$, $0.092 \div 0.138$, $0.138 \div 0.184$, $0.184 \div 0.230$ segments$/l^2$, as graphically illustrated in the inset. Polymers considered are 20-segment long, with $\sigma = l$, $D/l = 5.0$, and polymer-segment number density in solution is 0.225. (Colour version available online.)

here approximated as pseudo one-component systems, in which the colloid particles are treated as the pseudo pure component and polymer chains and solvent molecules are considered as a smeared continuum. The effect of polymers in solution is considered only through the effective colloid–colloid potential of mean force obtained through the simulations previously discussed.

Molecular van der Waals models are used to describe both the fluid and the solid phases at equilibrium. The reference fluid consists of the hard-sphere system described by Carnahan and Starling [41]. The random-phase approximation is applied to compute the Helmholtz free energy for the fluid phase. The free energy for the solid phase is obtained within a cell theory by considering the crystal as a perfect lattice [42]. The cell theory was considered through the improvement due to Velasco *et al.* [43] that yields a satisfactory agreement between simulation and theory for the free energy of hard-sphere solids [44]. For both phases the perturbation follows from the simulated pair potentials of mean force. Contributions due to three- (or higher-) body interactions to the free energy are neglected. By assuming that the same potential of mean force represents colloid–colloid interactions in all phases at equilibrium we imply that the polymer concentration is similar in all phases. This approximation is reasonable at low polymer concentrations, such as those considered

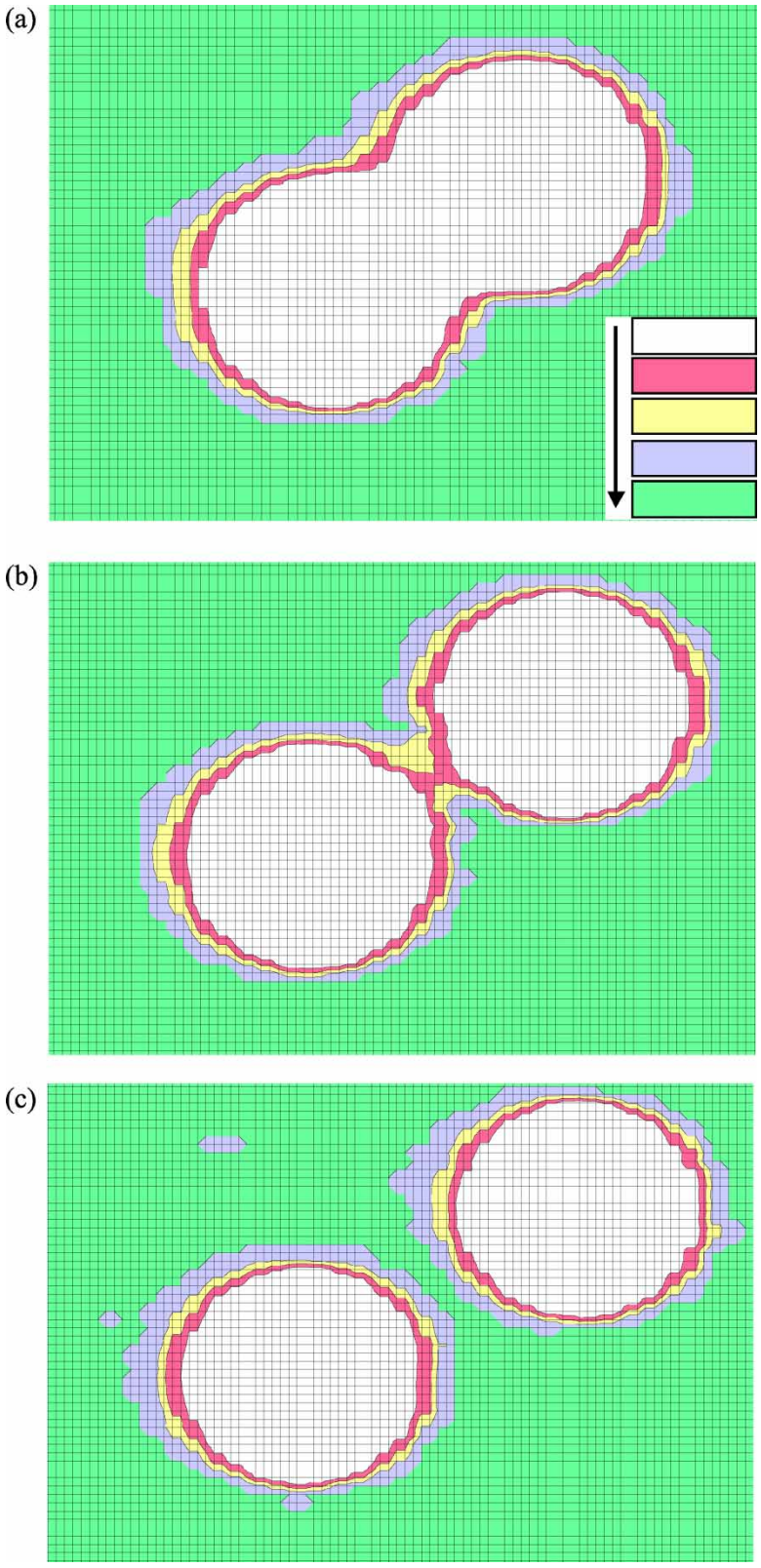

FIGURE 5 Polymer-segment density profiles around interacting pairs of $D = 5l$ colloids at colloid–colloid center-to-center separations $r/l = 5.1$ (a), 7.0 (b), and 8.0 (c). Different colors represent different surface densities in the range $0 \div 0.046$, $0.046 \div 0.092$, $0.092 \div 0.138$, $0.138 \div 0.184$, $0.184 \div 0.230$ segments$/l^2$, as graphically illustrated in the inset. Polymers considered are 20-segment long, with $\sigma = 1.2l$, and $\rho_p l^3 = 0.225$. (Colour version available online.)

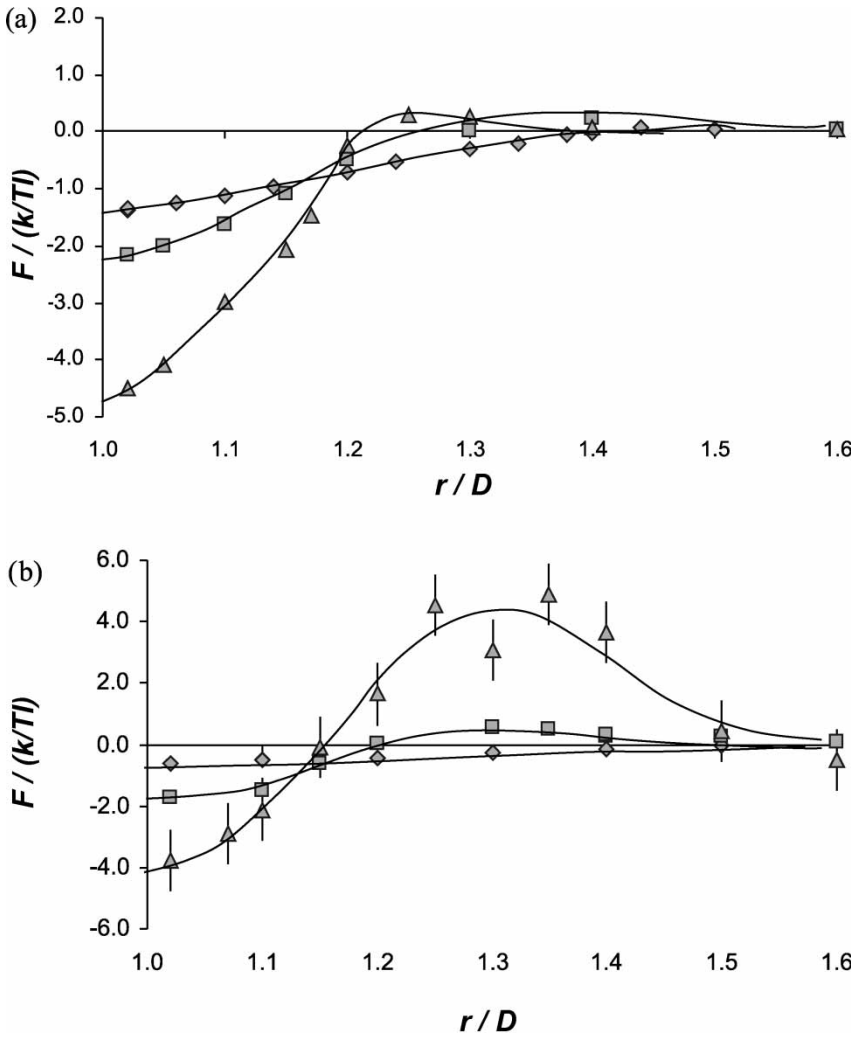

FIGURE 6 Colloid–colloid force for pairs of $D/l = 5$ colloids dissolved in 20-segment-long polymer solutions as a function of polymer concentration. (a) For $\sigma/l = 1.0$ polymers (diamonds are for $\rho_P l^3 = 0.225$, squares are for $\rho_P l^3 = 0.30$, triangles are for $\rho_P l^3 = 0.45$). (b) For $\sigma/l = 1.2$ polymers (diamonds are for $\rho_P l^3 = 0.10$, squares are for $\rho_P l^3 = 0.225$, triangles are for $\rho_P l^3 = 0.30$). Lines are guides for the eye.

here. More rigorous studies have been applied to directly assess the polymer/colloid composition of the two fluid phases at equilibrium either by molecular simulation [24] or by theoretical calculations [10]. Rather than investigating the composition of the two fluid phases in equilibrium, we are here more interested in understanding under which conditions a fluid–fluid rather than a fluid–solid demixing takes place in colloid/polymer mixtures. The compositions of different phases at equilibrium are obtained by imposing:

$$\tilde{T}_i = \tilde{T}_j \quad \tilde{P}_i = \tilde{P}_j \quad \tilde{\mu}_i = \tilde{\mu}_j, \tag{3}$$

where $\tilde{T}$, $\tilde{P}$, $\tilde{\mu}$ are reduced temperature ($\tilde{T} = kT/\varepsilon$), pressure ($\tilde{P} = \rho_C/\rho_C^0\varepsilon$), and chemical potential ($\tilde{\mu} = \mu/kT$). ρ_C^0 is the one-colloid density, ε, equal to 1 kT, is used to normalize all colloid–colloid interactions, and subscripts i and j stand for the two phases.

The perturbative colloid–colloid potential of mean force W^{pert} is obtained as the sum of a dispersive term W^{disp} responsible for van der Waals attractions, and a polymer-mediated term W^{pol} that approximates the simulated colloid–colloid effective interactions:

$$W^{\text{pert}}(\tilde{r}) = W^{\text{disp}}(\tilde{r}) + W^{\text{pol}}(\tilde{r}). \tag{4}$$

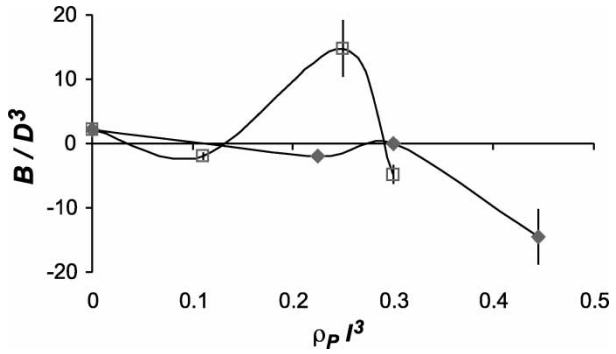

FIGURE 7 Colloid–colloid osmotic second virial coefficient B as a function of polymer-segment number density in solution. Diamonds are for $D = 5l$ colloids in 20-segment-long $\sigma = 1.0l$, squares are for $D = 5l$ colloids in 20-segment-long $\sigma = 1.2l$ polymer solutions. Data for the colloid–colloid potential of mean force are derived numerically from results shown in Fig. 6.

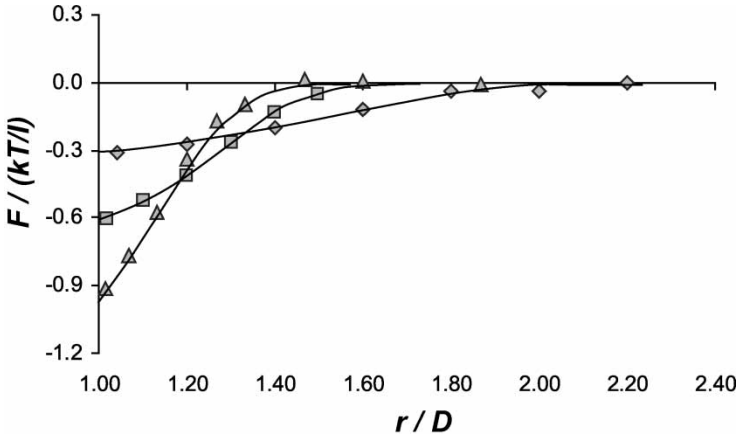

FIGURE 8 Colloid–colloid force as a function of center-to-center reduced separation for pairs of colloids in $\rho_P l^3 = 0.10$, $\sigma/l = 1.2$, 20-segment-long polymer solutions. Colloid particles of different sizes are considered. Diamonds are for $D/l = 2.5$, squares are for $D/l = 5.0$, and triangles are for $D/l = 7.5$. Lines are guides for the eye.

A pair of similar colloid particles in solution experiences an attractive potential due to dispersive interactions. An inverse-power potential that decays with the sixth power of the colloid–colloid center-to-center separation is used to describe these interactions:

$$W^{\text{disp}}(\tilde{r}) = U_1(\tilde{r}) = \begin{cases} \infty & \tilde{r} < 1 \\ \frac{-\varepsilon_1}{\tilde{r}^{n_1}} & \tilde{r} \geq 1 \end{cases} \tag{5}$$

In our calculations, ε_1 is 1 kT, and n_1 is 6. The polymer-mediated term W^{pol} is approximated as the sum of one attractive and one repulsive inverse-power potential:

$$W^{\text{pol}}(\tilde{r}) = U_2(\tilde{r}) + U_3(\tilde{r}), \tag{6}$$

where

$$U_2(\tilde{r}) = \begin{cases} \infty & \tilde{r} < 1 \\ \frac{-\varepsilon_2}{\tilde{r}^{n_2}} & \tilde{r} \geq 1 \end{cases}, \quad U_3(\tilde{r}) = \begin{cases} \infty & \tilde{r} < 1 \\ \frac{\varepsilon_3}{\tilde{r}^{n_3}} & \tilde{r} \geq 1 \end{cases}, \tag{7}$$

n_2, n_3, ε_2, and ε_3 are parameters representative of the range and of the strength of colloid–colloid interaction. These parameters are fitted to the simulated colloid–colloid potentials.

Reduced pressure and chemical potential for colloids in the fluid (Eqs. (8) and (9)) and in the solid phase (Eqs. (10) and (11)) are:

$$\frac{\tilde{p}_{\text{fluid}}}{\tilde{T}} = \eta_C \frac{1 + \eta_C + \eta_C^2 - \eta_C^3}{(1-\eta_C)^3} - \frac{1}{\tilde{T}}\frac{\varepsilon_1}{\varepsilon}\frac{12\eta_C^2}{(n_1-3)} + \frac{1}{\tilde{T}}\frac{\varepsilon_2}{\varepsilon}\frac{12\eta_C^2}{(n_2-3)} - \frac{1}{\tilde{T}}\frac{\varepsilon_3}{\varepsilon}\frac{12\eta_C^2}{(n_3-3)} \tag{8}$$

$$\tilde{\mu}_{\text{fluid}} = \ln\left(\rho_C^0 \Lambda^3\right) + \ln(\eta_C) + \frac{4\eta_C - 3\eta_C^2}{(1-\eta_C)^2} + \frac{1 + \eta_C + \eta_C^2 - \eta_C^3}{(1-\eta_C)^3} - \frac{1}{\tilde{T}}\frac{\varepsilon_1}{\varepsilon}\frac{24\eta_C}{(n_1-3)} + \frac{1}{\tilde{T}}\frac{\varepsilon_2}{\varepsilon}\frac{24\eta_C}{(n_2-3)} - \frac{1}{\tilde{T}}\frac{\varepsilon_3}{\varepsilon}\frac{24\eta_C}{(n_3-3)} - 1 \tag{9}$$

$$\frac{\tilde{p}_{\text{solid}}}{\tilde{T}} = \eta_C \frac{1}{1-\frac{1}{\tilde{R}}} - \eta_C \frac{Z_{\text{latt}} n_1}{6}\frac{1}{\tilde{T}}\frac{\varepsilon_1}{\varepsilon}\frac{1}{\tilde{R}^{n_1}} + \eta_C \frac{Z_{\text{latt}} n_2}{6}\frac{1}{\tilde{T}}\frac{\varepsilon_2}{\varepsilon}\frac{1}{\tilde{R}^{n_2}} - \eta_C \frac{Z_{\text{latt}} n_3}{6}\frac{1}{\tilde{T}}\frac{\varepsilon_3}{\varepsilon}\frac{1}{\tilde{R}^{n_3}} \tag{10}$$

$$\tilde{\mu}_{\text{solid}} = \ln\left(\rho_C^0 \Lambda^3\right) + \ln(\eta_C) - \ln(8) - 3\ln\left(1 - \frac{1}{\tilde{R}}\right) + \frac{1}{1-\frac{1}{\tilde{R}}} - \frac{Z_{\text{latt}}}{2\tilde{T}}\frac{\varepsilon_1}{\varepsilon}\frac{1}{\tilde{R}^{n_1}} - \frac{Z_{\text{latt}} n_1}{6\tilde{T}}\frac{\varepsilon_1}{\varepsilon}\frac{1}{\tilde{R}^{n_1}} + \frac{Z_{\text{latt}}}{2\tilde{T}}\frac{\varepsilon_2}{\varepsilon}\frac{1}{\tilde{R}^{n_2}} - \frac{Z_{\text{latt}} n_2}{6\tilde{T}}\frac{\varepsilon_2}{\varepsilon}\frac{1}{\tilde{R}^{n_2}} - \frac{Z_{\text{latt}}}{2\tilde{T}}\frac{\varepsilon_{31}}{\varepsilon}\frac{1}{\tilde{R}^{n_3}} - \frac{Z_{\text{latt}} n_3}{6\tilde{T}}\frac{\varepsilon_3}{\varepsilon}\frac{1}{\tilde{R}^{n_3}} \tag{11}$$

η_C is the packing fraction of colloids in solution ($\eta_C = \pi\rho_C D^3/6$), ρ_C is the colloid number density, Λ is the thermal wavelength, Z_{latt} is the coordination number of the lattice assumed for the solid, and $\tilde{R}$ is the center-to-center distance between colloids in the solid phase. Assuming that the solid phase is a perfect crystal, $\tilde{R}$ is a function of the colloid number density in the solid and of the close-packed density, ρ_C^{cp}, of the crystal considered:

$$\tilde{R} = \left(\frac{\rho_C}{\rho_C^{\text{cp}}}\right)^{-1/3} = \left(\frac{\eta_C}{\eta_C^{\text{cp}}}\right)^{-1/3}. \tag{12}$$

The close-packed packing fraction η_C^{cp} equals 0.74048 for $Z_{\text{latt}} = 12$ (face-centered cubic unit cell) and 0.6800 for $Z_{latt} = 8$ (body-centered cubic unit cell).

Fluid–fluid and fluid–solid phase coexistence curves for $D = 5l$ colloids in solution with no polymer, 10-segment-long, $\sigma = l$, $\rho_P l^3 = 0.30$

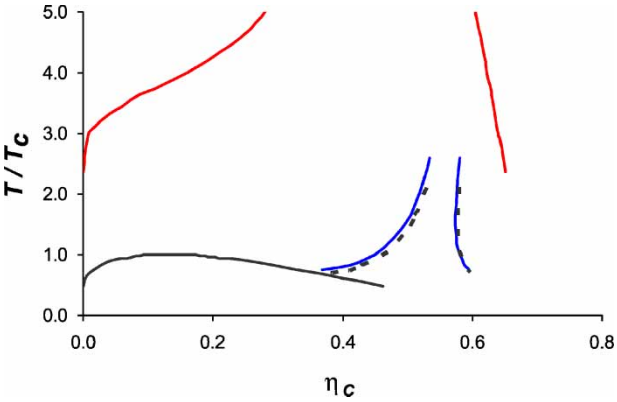

FIGURE 9 Global phase diagram for $D = 5l$ colloids in polymer solution. Continuous line is for fluid–fluid phase coexistence; black dotted lines are for fluid–solid phase coexistence when no polymers are in solution; blue and red lines are for fluid–solid coexistence curves for colloids in $\rho_P l^3 = 0.10$, 30-segment-long and in $\rho_P l^3 = 0.30$, 10-segment-long polymer solutions, respectively. Temperature is reduced by the fluid–fluid critical temperature T_C. Lattice coordination number for the crystal is $Z_{\text{latt}} = 8$. Colloid–colloid potentials of mean force are from results shown in Fig. 1. (Colour version available online.)

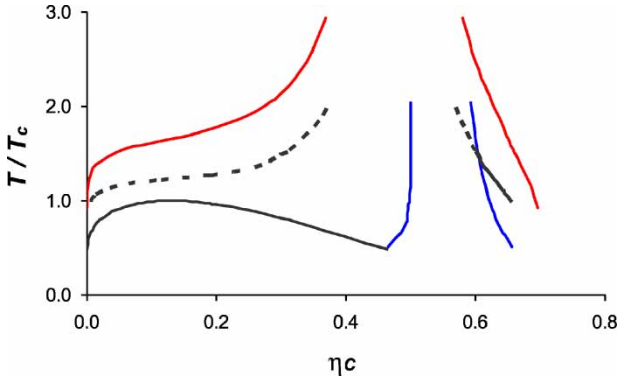

FIGURE 10 Global phase diagram for colloids in $\sigma = 1.2l$, $\rho_P l^3 = 0.10$, 20-segment-long polymer solution. Continuous line is for fluid–fluid phase coexistence; black dotted lines are for fluid–solid phase coexistence when no polymers are in solution; blue and red lines are for fluid–solid coexistence curves for $D = 2.5l$ and $D = 7.5l$ colloids, respectively. Temperature is reduced by the fluid–fluid critical temperature T_C. Lattice coordination number for the crystal is $Z_{\text{latt}} = 12$. Colloid–colloid potentials of mean force are from results shown in Fig. 8. (Colour version available online.)

polymers, and 30-segment-long, $\sigma = l$, $\rho_P l^3 = 0.10$ polymers are shown in Fig. 9. The lattice coordination number for the solid is $Z_{\text{latt}} = 8$. When no polymers are in solution, the van der Waals model predicts a fluid–fluid coexistence curve that lies at lower packing fraction compared to the fluid–solid coexistence curve. Because the range of the polymer-mediated colloid–colloid depletion potential is short at the conditions considered in Fig. 9 (potentials are derived from simulation results shown in Fig. 1), as polymers are dissolved in solution, the fluid–solid coexistence curve is shifted at higher reduced temperatures. However, while the fluid–fluid coexistence curve is stable when 30-segment-long polymers are in solution, it becomes metastable when 10-segment-long polymers are added to the system. Our results show that as the intensity of the depletion attraction at contact increases, the fluid–fluid coexistence curve may become metastable depending on the range of the polymer-mediated colloid–colloid potential of mean force. In particular, small amounts of short polymers can have a dramatic effect on the features of the phase diagrams for colloids.

Fluid–fluid and fluid–solid coexistence curves for colloids in 20-segment-long, $\sigma = 1.2l$, $\rho_P l^3 = 0.10$ polymer solution are shown in Fig. 10. Colloids considered have different diameters: $D = 2.5l$ or $7.5l$. For comparison, predictions for the phase diagram of colloidal systems in the absence of polymers in solution are also shown in Fig. 10. The coordination number assumed for the crystal is $Z_{\text{latt}} = 12$. Under the conditions considered in Fig. 10, when no polymers are in solution the fluid–fluid coexistence curve is metastable with respect to the fluid–solid coexistence curve. When small colloids are dissolved in polymer solution, because of long-range polymer-mediated colloid–colloid depletion interactions, the fluid–fluid coexistence region becomes stable with respect to the fluid–solid coexistence curve. Vice versa, when large colloids are dissolved in short polymer solutions at similar conditions, because of short-ranged depletion interactions, the fluid–solid coexistence curve is shifted at higher reduced temperatures, and the fluid–crystal coexistence region is expanded. Our results qualitatively agree with experimental results for PMMA spheres in solutions containing low- or high-molecular-weight polystyrene [13].

CONCLUSIONS

Effective interactions were computed by Monte Carlo simulations in the canonical ensemble between pairs of hard-sphere colloid particles dissolved in freely-jointed-hard-spheres polymer solutions. Polymers considered were 10-, 20-, or 30-segment long and characterized by different flexibility. The size of the interacting colloid particles was similar to or smaller than the radius of gyration of the polymers.

Pairs of colloid particles in polymer solution experience a depletion attraction that may be coupled with mid-range colloid–colloid repulsion when concentrated solutions of short rigid polymers are considered. The depletion attraction is long-ranged when colloids are dissolved in solutions containing long polymers. As polymer concentration increases, the depletion attraction at contact increases, but the range of the interaction decreases.

Simulated forces were used to compute the osmotic second virial coefficient for colloids.

In qualitative agreement with available experimental data, our results indicate that the depletion term of the osmotic second virial coefficient follows a non-monotonic behavior as polymer concentration increases. Simulated pair potentials were used, within a perturbation theory, to predict fluid–fluid and fluid–solid coexistence curves for colloid particles in polymer solutions. The customary phase diagram is predicted when colloids are dissolved in solutions containing long flexible polymers, but as the polymer concentration increases, the polymer length decreases, and/or the polymer stiffness increases, the fluid–fluid coexistence curve may become metastable with respect to the fluid–solid coexistence region.

Acknowledgements

The quality of the manuscript has significantly improved during the revision process through helpful and instructive discussions with Prof. S.A. Egorov, University of Virginia. Partial support for this work was provided by D.O.E. under contract No DE-FG02-98ER-14847. The authors acknowledge interesting and instructive discussions with J.M. Prausnitz, and C.K. Hall. A.S. thanks R. Wimberly for encouragement and support. All calculations were performed in computers provided by the University of Padova through a 'Progetto di Ricerca per Giovani Ricercatori' grant.

References

[1] Hiemenz, P.C. and Rajagopalan, R. (1997) *Principles of Colloid and Surface Chemistry*, 3rd Ed. (Marcel Dekker, New York).
[2] Jenkins, P. and Snowden, M. (1996) "Depletion flocculation in colloidal dispersions", *Adv. Colloid Interface Sci.* **68**, 57–96.
[3] Asakura, S. and Oosawa, F. (1954) "On interaction between two bodies immersed in a solution of macromolecules", *J. Chem. Phys.* **22**, 1255.
[4] Asakura, S. and Oosawa, F. (1958) "Interaction between particles suspended in solutions of macromolecules", *J. Polym. Sci.* **33**, 183.
[5] de Hek, H. and Vrij, A. (1981) "Interactions in mixtures of colloidal silica spheres and polystyrene molecules in cyclohexane. I. Phase separation", *J. Colloid Interface Sci.* **84**, 409.
[6] Sperry, P.R., Hopfenberg, H.B. and Thomas, N.L. (1981) "Flocculation of latex by water-soluble polymers: experimental confirmation of a nonbridging, nonadsorptive volume-restriction mechanism", *J. Colloid Interface Sci.* **82**, 62–76.
[7] Joanny, J.F., Leibler, L. and de Gennes, P.G. (1979) "Effects of polymer solutions on colloid stability", *J. Polym. Sci.: Polym. Phys. Ed.* **17**, 1073–1084.
[8] Fleer, G.J., Scheutjens, J.M.H.M. and Cohen Stuart, M.A. (1988) "Theoretical progress in polymer adsorption, steric stabilization and flocculation", *Colloids Surf.* **31**, 1–29.
[9] Yethiraj, A., Hall, C.K. and Dickman, R. (1992) "Interactions between colloids in solutions containing dissolved polymer", *J. Colloid Interface Sci.* **151**, 102–117.
[10] Paricaud, P., Varga, S. and Jackson, G. (2003) "Study of the demixing transition in model athermal mixtures of colloids and flexible self-excluding polymers using the thermodynamic perturbation theory of Wertheim", *J. Chem. Phys.* **118**, 8525–8536.
[11] Ye, X., Narayanan, T., Tong, P., Huang, J.S., Lin, M.Y., Carvalho, B.L. and Fetters, L.J. (1996) "Depletion interactions in colloid-polymer mixtures", *Phys. Rev. E* **54**, 6500–6510.
[12] Poon, W.C.K. (2002) "The physics of a model colloid-polymer mixture", *J. Phys.: Condens. Matter* **14**, R859.
[13] Ilett, S.M., Orrock, A., Poon, W.C.K. and Pusey, P.N. (1995) "Phase behavior of a model colloid-polymer mixture", *Phys. Rev. E* **51**, 1344–1352.
[14] Kulkarni, A.M., Chatterjee, A.P., Schweizer, K.S. and Zukoski, C.F. (1999) "Depletion interaction in the protein limit: effects of polymer-density fluctuations", *Phys. Rev. Lett.* **83**, 4554–4557.
[15] Kulkarni, A.M., Chatterjee, A.P., Schweizer, K.S. and Zukoski, C.F. (2000) "Effects of polymer density fluctuations on depletion interactions", *J. Phys.: Condens. Matter* **12**, A301–A307.
[16] Kulkarni, A.M., Chatterjee, A.P., Schweizer, K.S. and Zukoski, C.F. (2000) "Effects of polyethylene glycol on protein interactions", *J. Chem. Phys.* **113**, 9863–9873.
[17] Kulkarni, A. and Zukoski, C. (2001) "Depletion interactions and protein crystallization", *J. Cryst. Growth* **232**, 156.
[18] McMillan, W.G. and Mayer, J.E. (1945) "The statsitical thermodynamics of multicomponent systems", *J. Chem. Phys.* **13**, 276.
[19] Prausnitz, J.M., Lichtenthaler, R.M. and de Azevedo, E.G. (1999) *Molecular Thermodynamics of Fluid-Phase Equilbria*, 3rd Ed. (Prentice Hall, New Jercy).
[20] Gast, A.P., Hall, C.K. and Russel, W.B. (1983) "Polymer-induced phase separations in nonaqueous colloidal suspensions", *J. Colloid Interface Sci.* **96**, 251–267.
[21] Dickman, R. and Yethiraj, A. (1994) "Polymer-induced forces between colloidal particles. A Monte Carlo simulation", *J. Chem. Phys.* **100**, 4683–4690.
[22] Louis, A.A., Bolhuis, P.G., Meijier, E.J. and Hansen, J.P. (2002) "Polymer-induced depletion potentials in polymer-colloid mixtures", *J. Chem. Phys.* **117**, 1893–1907.
[23] Dzubiella, J., Likos, C.N. and Lowen, H. (2002) "Phase behavior and structure of star-polymer-colloid mixtures", *J. Chem. Phys.* **116**, 9518–9530.
[24] Bolhuis, P.G., Meijer, E.J. and Louis, A.A. (2003) "Colloid-polymer mixtures in the protein limit", *Phys. Rev. Lett.* **90**, 068304/1.
[25] Allen, M.P. and Tildesley, D.J. (1987) *Computer Simulation of Liquids* (Oxford Science Publications, Claredon Press, Oxford).
[26] Lal, M. (1969) "'Monte Carlo' computer simulation of chain molecules", *Mol. Phys.* **17**, 57.
[27] Verlet, L. (1967) "Computer "experiments" on classical fluids. I. Thermodynamical properties of Lennard-Jones molecules", *Phys. Rev.* **159**, 98.
[28] Wu, J.Z., Bratko, D., Blanch, H.W. and Prausnitz, J.M. (1999) "Monte Carlo simulation for the potential of mean force between ionic colloids in solutions of asymmetric salts", *J. Chem. Phys.* **111**, 7084–7096.
[29] Garel, T. and Oral, H. (1990) "Guided replication of random: a new Monte Carlo method", *J. Phys. A: Math. Gen.* **23**, L621–L626.
[30] Higgs, P.Q. and Orland, H. (1991) "Scaling behavior of polyelectrolytes and polyampholities: simulation by an ensemble growth method", *J. Chem. Phys.* **95**, 4506–4518.
[31] Striolo, A., Bratko, D., Prausnitz, J.M., Elvassore, N. and Bertucco, A. (2001) "Influence of polymer structure upon active-ingredient loading: a Monte Carlo simulation study for design of drug-delivery devices", *Fluid Phase Eq.* **183-184**, 341–350.
[32] Dickman, R., Attard, P. and Simonian, V. (1997) "Entropic forces in binary hard sphere mixtures: theory and simulation", *J. Chem. Phys.* **107**, 205–213.
[33] Striolo, A. and Prausnitz, J.M. (2001) "Adsorption of branched homopolymers on a solid surface", *J. Chem. Phys.* **114**, 8565–8572.
[34] Chen, Y.-L. and Schweizer, K.S. (2002) "Depletion interactions in suspensions of spheres and rod-polymers", *J. Chem. Phys.* **117**, 1351–1362.
[35] Mao, Y., Gates, M.E. and Lekkerkerker, H.N.W. (1995) "Depletion stabilization by semidilute rods", *Phys. Rev. Lett.* **75**, 4548–4551.

[36] Pham, K., Puertas, A.M., Bergenholtz, J., Egelhaaf, S.U., Moussaïd, A., Pusey, P.N., Schofield, A.B., Cates, M.E., Fuchs, M. and Poon, W.C.K. (2002) "Multiple glassy states in a simple model system", *Science* **296**, 104.
[37] Poon, W.C.K., Selfe, J.S., Robertson, M.B., Ilett, S.M., Pirie, A.D. and Pusey, P.N. (1993) "An experimental study of a model colloid-polymer mixture", *J. Phys. II (Paris)* **3**, 1075.
[38] Bergenholtz, J., Poon, W.C.K. and Fuchs, M. (2003) "Gelation in model colloid-polymer mixtures", *Langmuir* **19**, 4493.
[39] Tuinier, R., Vliegenthart, G.A. and Lekkerkerker, H.N.W. (2000) "Depletion interaction between spheres immersed in a solution of ideal polymer chains", *J. Chem. Phys.* **113**, 10768–10775.
[40] Chatterjee, A.P. and Schweizer, K.S. (1998) "Correlation effects in dilute particle-polymer mixtures", *J. Chem. Phys.* **109**, 10464–10476.
[41] Carnahan, N.F. and Starling, K.E. (1969) "Equation of states for nonattracting rigid spheres", *J. Chem. Phys.* **51**, 635–636.
[42] Daanoun, A., Tejero, C.F. and Baus, M. (1994) "Van der Waals theory for solids", *Phys. Rev. E* **50**, 2913–2924.
[43] Velasco, E., Mederos, L. and Navascues, G. (1998) "Phase diagram of colloidal systems", *Langmuir* **14**, 5652–5655.
[44] Wu, J. and Prausnitz, J. (2000) "Phase equilibria in a system of "breathing" molecules", *Fluid Phase Eq.* **194–197**, 689–700.